Biomaterials Science

ROYAL SOCIETY OF CHEMISTRY

REVIEW

View Article Online
View Journal | View Issue

Cite this: *Biomater. Sci.*, 2024, **12**, 4650

Lanthanide-doped upconversion nanoparticles as nanoprobes for bioimaging

Hengde Li, [a] Haitao Liu, [a] Ka-Leung Wong *[b] and Angelo H. All *[a]

Upconversion nanoparticles (UCNPs) are a class of nanomaterials composed of lanthanide ions with great potential for paraclinical applications, especially in laboratory and imaging sciences. UCNPs have tunable optical properties and the ability to convert long-wavelength (low energy) excitation light into short-wavelength (high energy) emission in the ultraviolet (UV)-visible and near-infrared (NIR) spectral regions. The core–shell structure of UCNPs can be customized through chemical synthesis to meet the needs of different applications. The surface of UCNPs can also be tailored by conjugating small molecules and/or targeting ligands to achieve high specificity and selectivity, which are indispensable elements in biomedical applications. Specifically, coatings can enhance the water dispersion, biocompatibility, and efficiency of UCNPs, thereby optimizing their functionality and boosting their performance. In this context, multimodal imaging can provide more accurate *in vivo* information when combined with nuclear imaging. This article intends to provide a comprehensive review of the core structure, structure optimization, surface modification, and various recent applications of UCNPs in biomolecular detection, cell imaging, tumor diagnosis, and deep tissue imaging. We also present and discuss some of their critical challenges, limitations, and potential future directions.

Received 6th June 2024,
Accepted 5th August 2024

DOI: 10.1039/d4bm00774c

rsc.li/biomaterials-science

1. Introduction

Rare earth (RE) elements are a group of 17 metal chemical elements that include scandium (Sc), yttrium (Y), and fifteen lanthanides (Lns), which have a 4f electronic configuration and usually undergo f–f electronic transitions. Ln elements numbered 57 to 71 in the periodic table have similar chemical properties. Neodymium (Nd), holmium (Ho), erbium (Er), thulium (Tm), and ytterbium (Yb) are commonly used to synthesize Ln-doped upconversion nanoparticles (UCNPs), which can convert near-infrared (NIR) excitation into programmable ultraviolet (UV)-visible emission through a nonlinear process. During upconversion processes, photons emitted by UCNPs have a higher energy than those absorbed. This energy difference is known as the anti-Stokes shift.[1]

UCNPs are typically composed of three parts: a host matrix, activators, and sensitizers. The host matrix is the material that forms the bulk of the nanoparticle,[2] with examples including $NaREF_4$ (RE = rare earth), CaF_2, and Y_2O_3. The host matrix provides a lattice structure for the activator and sensitizer ions.[3] Activators, such as Er^{3+} and Tm^{3+}, are embedded in the host matrix absorbing low-energy photons and emitting high-energy photons through upconversion. Sensitizers are often co-doped into UCNPs to absorb excited radiation and transfer the energy to the activator. It is known that during the process of synthesis, the concentration of activator ions in host lattices must be carefully controlled to avoid cross-relaxation and maintain high upconversion efficiency. Increasing the sensitizer ion concentration in UCNPs can improve the photon absorption capacity, thus enhancing the upconversion luminescence (UCL).[4] However, beyond a certain threshold (1–5 mol%), any further increase in the sensitizer ion concentration will result in a significant decrease in the luminescence intensity.[5] This phenomenon is commonly known as "concentration quenching".[6] In addition, increasing the concentration of lanthanide ion doping in UCNPs can result in a more intricate energy transfer process within the particles, leading to a higher dissipation of energy towards the surface, and this phenomenon is commonly referred to as surface quenching. The concentration quenching effect is also closely coupled to surface quenching.[5] Due to surface quenching and concentration quenching, the quantum yield (QY) of UCNPs is low. Nevertheless, different core–shell structures are designed to improve both the UCL intensity and the QY of UCNPs. Inert shells, such as $NaYF_4$, $NaGdF_4$, or CaF_2, can passivate the surface defects and reduce surface quenching. On the other hand, active shells could be constructed to disperse higher sensitizer concentrations in different layers and reduce concentration quenching.[7,8] Concurrently, constructing core–shell

[a]*Department of Chemistry, Hong Kong Baptist University, 224 Waterloo Road, Kowloon, Hong Kong SAR 999077, China. E-mail: angelo@hkbu.edu.hk*
[b]*Department of Applied Biology and Chemical Technology, The Hong Kong Polytechnic University, Hong Kong SAR 999077, China*

structures is also a way to enhance their biological applications. For instance, through typical Stober-based surface modification, the direct introduction of primary amine groups on the surface of UCNPs enables their modifications with water-soluble targeting ligands.[9]

The species and dopant concentration ratio of guest ions are also crucial in controlling the wavelength and intensity of the emitted light in UCNPs. Usually, Yb^{3+} is added as a sensitizer to these combinations to absorb the pump photon produced by a 980 nm laser and transfer it to the activators, such as Er^{3+}, Eu^{3+}, Tm^{3+}, or Ho^{3+}, which emit light with the stipulated desired wavelength (Fig. 1).[10] Another commonly used sensitizer is Nd^{3+}, with an efficient absorption band at ~808 nm. Compared with the Yb^{3+} ion sensitization system, Nd^{3+} uses an 808 nm laser as the excitation light source, which reduces the undesired photothermal effect of the 980 nm laser, a practical consideration that is critical to improve the feasibility of biological applications.[11] In addition, the use of dye-sensitized UCNPs is an excellent strategy for improving their quantum yield and upconversion efficiency.

This is because common industrial NIR dyes have a high extinction coefficient. For example, the extinction coefficient of the near-infrared dye IR-806 is about $\sim 5 \times 10^6$ times higher than that of $NaYF_4$:Yb/Er. By using near-infrared dyes as "antennas", near-infrared photons are efficiently absorbed and transferred to the excited state of lanthanide ions through a resonance energy transfer process, thus enhancing the emission intensity.[12]

Organic fluorescent probes have the advantages of a wide range of excitation and emission wavelengths, structural diversity, and strong flexibility, making them ideal fluorescent probes for biological imaging. However, traditional organic fluorescent probes are limited in their applications *in vivo* primarily because they typically need to be excited using relatively short wavelength light (such as ultraviolet) to emit longer wavelength light (such as visible light). This optical property restricts the application of organic fluorescent probes in deep tissue imaging because the penetration depth of ultraviolet and visible light is relatively shallow. Moreover, long-term exposure to short UV excitation wavelengths could cause irreversible cell damage.[13] Due to their outstanding optical properties, quantum dots (QDs), including metal sulfide QDs and metal halide perovskite QDs, have become a potential bioimaging technology. However, the inherent heavy metal content and toxicity of quantum dots limit their biological applications. Although an inorganic shell or a polymer coating can be introduced on the core material to protect it from slow degradation, the toxic metal ions released by these nanoprobes still seriously threaten the physiological environment due to photooxidation or poor stability.[14]

UCNP-based nanoprobes have shown higher potential in bioimaging than traditional fluorescent materials due to their superior physicochemical properties, such as a large anti-Stokes shift, excellent photostability, and long excited state lifetime.[15] Such nanoprobes can be functionalized to detect small organic molecule biomarkers, practically making them ideal bio-sensors.[16] UCNPs are widely used in super-resolution microscopy as fluorescent probes, and their small size and high emission intensity enable their use in the observation of subcellular structures and biomolecular dynamics.[17] UCNPs are also used for high-resolution imaging to visualize and track cellular structures and functions.[18] For cancer diagnosis, UCNPs provide a powerful platform for tumor cell detection with the ability to regulate size through synthesis and reduce non-specific binding through surface modification. In addition, selective UCNP surface modification with antibodies or ligands enables high-contrast imaging of tumor cells.[15,19] Previous studies have shown that UCNPs can be used to detect blood-based biomarkers, offering potential applications for cancer diagnosis.[20] UCNPs can also be developed for multiple applications, including diagnostics and therapy. In photodynamic therapy, UCNPs can act as photosensitizers, absorbing external light excitation and transferring energy to produce reactive oxygen species that could destroy tumor cells or other diseased tissues. They can also be used as drug carriers for bioimaging therapeutics or genes (such as doxorubicin, siRNA, DNA, and microRNA) or photosensitizers.[21]

The long wavelength excitation light of UCNPs avoids tissue autofluorescence interference, allowing for deep tissue penetration of up to a few centimeters, which enables the visualization of living organisms' structures and functions by imaging techniques.[17,22,23] Understandably, UCNP probes for multimodal imaging can be constructed.[24] Yb^{3+} and Gd^{3+}-doped UCNPs can be used as contrast agents for computed tomography (CT) imaging due to their high atomic number and strong X-ray attenuation properties.[25] Similarly, Gd-based UCNPs are suitable for magnetic resonance imaging (MRI) applications. This is attributed to the unpaired 4f electrons in Gd^{3+} ions. These unpaired electrons generate strong magnetic moments that can interact with nearby water protons, accelerating the relaxation of water protons and leading to contrast enhancement in T_1-weighted MRI scans.[26] This approach offers high accuracy, high resolution, and low invasiveness, enabling comprehensive acquisition of imaging signals (both structural and functional) at the molecular levels.[27,28] Due to their NIR excitation properties, UCNPs could effectively and selectively be excited even in deeper structures of biological tissues, allowing for deep tissue imaging. This in turn will lead to clinically

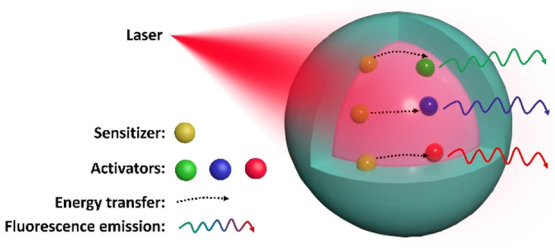

Fig. 1 Schematic of the UCNP design, showing NIR light absorbed by the sensitizer and energy transferred to an activator, emitting luminescence with a specific wavelength.

improved diagnostic accuracy, a critical step in early tumor detection.[12,29] In neuro-imaging applications, peptides on the surface of UCNPs could be modified to enhance their blood–brain barrier (BBB) permeability, allowing them to even target specific neurons in the brain.[30] Customized UCNPs were shown to act as optogenetic actuators of transcranial near-infrared light to stimulate deep brain neurons.[31] Research on UCNPs in the field of bioimaging has been gradually translated into clinical applications. By using the real-time signal provided by UCNPs, upconversion emission with visible intensity is designed to realize clinical applications, such as guided surgical resection. This technology can help doctors pinpoint lesions and improve surgical accuracy, thereby improving patient outcomes and survival rates. As research on the use of UCNPs in bioimaging and clinical applications continues to deepen, it is believed that UCNPs will play a broader role in the medical field and bring about more innovation and progress in clinical practice.[32]

This paper reviews the application of UCNPs in bioimaging for disease diagnosis at the micro- and macro-levels. At the micro-level, UCNPs can be used for biomolecular detection and cell imaging, helping researchers observe the biomolecular interactions and cell structures within cells, such as the detection and analysis of cancer cells. At the macro-level, UCNPs can also be employed for deep tissue imaging, penetrating deep into tissues to observe the structure and function of entire organs, aiding in the diagnosis of organ diseases such as tumors, vascular diseases, central nervous system diseases, *etc*.

2. Upconversion mechanisms

In contrast to Stokes luminescence, where low energy (long wavelength) light is emitted upon absorption of high energy (short wavelength) light, UCNPs convert low energy excitation to high energy emission. For instance, Ln-doped UCNPs involve an Ln ion absorbing two or more photons to transition to an excited (E) state, which then relaxes to the ground (G) state and generates a photon with higher energy.[33] The basic upconversion emission mechanism can be divided into five categories: (a) excited state absorption (ESA), (b) energy transfer upconversion (ETU), (c) photon avalanche (PA), (d) cooperative sensitization upconversion (CSU), and (e) energy migration-mediated upconversion (EMU) (Fig. 2).

As the most basic mechanism in upconversion emission, in the ESA process, the Ln ion absorbs two photons in succession and gradually elevates to the E state (G → E1 → E2), and following radiation relaxation it comes back to the G state, achieving upconversion emission (Fig. 2a). Some Ln ions with ladder-level structures, such as Er^{3+}, Tm^{3+}, Ho^{3+}, and Nd^{3+}, exhibit efficient ESA, which can be excited by NIR lasers at 980 or 808 nm.[34] Unlike ESA, the energy transfer process of the ETU mechanism involves two adjacent Ln ions. In ETU, ion 1 as a sensitizer is excited (G → E1) by absorbing pump photons. The harvested energy is then transferred to its G state and activates the activator (ion 2). Sustained energy transfer excites ion 2 to its E2 state. Then the radiation returns to the G state, releasing higher energy photons (Fig. 2b). In most cases, UCNPs with different ion combinations, such as Yb^{3+}/Er^{3+}, Yb^{3+}/Tm^{3+}, and Yb^{3+}/Ho^{3+}, follow the ETU mechanism.[35] However, in the PA mechanism, an excited ion relaxes back to the G state by radiation, which excites a neighboring ion to the E2 state. These excited ions again relax back to the G state by radiation, which will excite more ions. This process is repeated, causing more and more ions to participate in the upconversion emission, resulting in an exponential increase in the number of photons emitted (Fig. 2c). The PA-based upconversion process provides the highest upconversion efficiency. Tm^{3+}-doped UCNPs have been successfully used in super-resolution imaging.[36] Meanwhile the CSU mechanism usually involves two ions (ion 1 and ion 3) of the same species absorbing pump photons and then cooperatively transferring harvested energy to ion 2 and exciting ion 2 to E2. The relaxation of ion 2 from E2 to the G state results in upconversion (Fig. 2d). And distinctively, the EMU process requires a core–shell structure with four types of lanthanide ions: sensitizer, accumulator, migrator, and activator (Fig. 2e). In this case, sequential energy transfers occur from the accumulator to the activator, producing UCL. Obviously, by adjusting the composition and concentration of dopant ions, the relative intensity of different emission peaks can be well-controlled and thus the emission wavelength of UCNPs will be manageable.

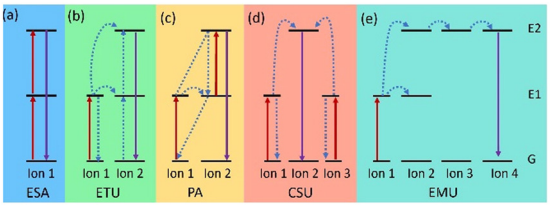

Fig. 2 Principal upconversion processes for lanthanide-doped UCNPs: (a) excited-state absorption (ESA), (b) energy transfer upconversion (ETU), (c) photon avalanche (PA), (d) cooperative sensitization upconversion (CSU), and (e) energy migration-mediated upconversion (EMU). The red, broken blue, and violet lines represent photon excitation, energy migration, and emission processes, respectively.

3. Bioimaging applications

Ln-doped UCNPs show high potential in biological imaging due to their advantages, such as narrow emission bandwidth, deep tissue penetration, and biocompatibility.

The applications of UCNPs in bioimaging are mainly divided into four parts:

(1) Biomolecular detection: by utilizing the unique luminescence mechanism and surface modification technology of UCNPs, which can detect biomolecules (such as proteins, DNA, H_2S, metal ions, *etc*.) with high sensitivity.

(2) Cell imaging: after UCNPs are modified for active uptake by cells, non-invasive imaging of the structure and function of cells can be performed.

(3) Cancer diagnosis and treatment: by exploiting the advantages of UCNPs in photonics and thermal applications, they can be used for early diagnosis, localization, and even in some cases, cancer treatment.

(4) Deep tissue imaging: by exploiting multimodal imaging techniques such as MRI and PET combination, UCNPs are modified and transplanted *in vivo*, enabling highly sensitive deep tissue imaging.[37,38]

3.1 Biomolecular detection

Recently, many small molecular biomarkers have been identified as indicators of physiological and pathological states *in vitro* and *in vivo*. For instance, glucose levels are markers for diabetes, cardiovascular disease, and cerebrovascular disease;[16] hydrogen sulfide (H_2S) is used to diagnose inflammatory diseases;[39] the hydroxyl radical ($^{\bullet}OH$) reflects the acid–base balance in the body and can be used to evaluate renal function and metabolism;[40] and hypochlorous acid (HOCl) is a reliable indicator of neuroinflammation.[41] Monitoring small molecular biomarkers is essential for early diagnosis, understanding disease progression, and evaluating the efficacy of ongoing treatment. Thanks to their unique optical properties, UCNPs have emerged as promising tools for monitoring diseases with small molecules as markers. In addition, UCNPs can also be used to detect drug residues, providing detection tools for food safety and environmental protection.[42]

Glucose is a vital biomolecule, used mainly for energy production and as an intermediary in many metabolism processes.[43,44] Therefore, accurate measurement of glucose concentration is crucial for clinical diagnosis. Shuai Zha *et al.* studied an "off–on" UCNP-nanoprobe $NaGdF_4$:Yb,Er@Ag anchored with glucose oxidase (GOx) for glucose detection. The fluorescence of the $NaGdF_4$:Yb,Er core is suppressed by the encapsulation of a thin argentum (Ag) shell. When GOx catalyzes glucose, it produces hydrogen peroxide (H_2O_2), which causes the dense Ag shell to disintegrate and release a fluorescence signal. This phenomenon is known as "fluorescence switching". The nanoprobe exhibits high sensitivity to even low glucose concentrations *in vitro*, with detection limits as low as 1.77 μM.[16]

Similarly, hydrogen sulfide (H_2S) is an important signaling molecule with various physiological and pathological effects in several diseases due to its antioxidant and anti-inflammatory effects. Accurate measurement of H_2S concentration can serve as a biomarker for evaluating human health status and predicting disease risk.[45,46] Liu's group developed two types of dye–UCNP probes for H_2S detection based on the luminescence resonance energy transfer (LRET) phenomenon. In this process, energy is transferred from a photosensitive upconversion material (the donor) to another organic dye (the acceptor) through non-radiative dipole–dipole interactions, resulting in the quenching of the UCL of UCNPs. Upon reacting with H_2S, the dye absorption decreases, inhibiting the LRET process, which leads to changes in the fluorescence wavelength or intensity that can be observed and measured. This approach can achieve highly sensitive and selective detection, making it a promising tool in biomedical research and clinical diagnostics. Practically, they developed a core–shell structured UCNP with $NaYbF_4$:Gd@$NaYF_4$:Yb,Tm as the energy donor and covalently coupled fluorescein derivative (Fl-1) on its surface as the energy acceptor for H_2S detection. H_2S can react with FI-1, transforming its five-membered ring into a six-membered ring (FI-2), inhibiting the LRET process and enhancing the UCL. This novel UCNP was successfully tested to determine the concentration of H_2S *in vitro* and *in vivo* (zebrafish and mouse models). As a result, they can be implemented in diagnosing arthritis and H_2S-associated tumors.[39]

Similarly, Liu's group assembled dyes (SiR1) and UCNPs ($NaYbF_4$:Gd@$NaYF_4$:Yb,Er) *via* hydrophobic–hydrophobic interactions to form SiR1–UCNP nanoprobes for hydrogen polysulfide (H_2S_n) detection, which is derived from H_2S. This nanoprobe can dynamically monitor the concentration changes of H_2S in living cells (*in vitro*) and mouse models (*in vivo*) with liver inflammation or damage.[47] These nanoprobes have potential applications in diagnosing and monitoring various diseases associated with H_2S, such as colorectal cancer, neurodegenerative diseases such as Alzheimer's disease, and hypertension.[48]

In addition, Liu's group developed an HOCl-activatable UCNP-nanoprobe for real-time detection of inflammation in the nervous system. HOCl is a reactive oxygen species (ROS) produced by activated microglia, which plays a crucial role in neuroinflammation. This unique UCNP-based nanoprobe can enable specific and sensitive imaging of neuroinflammation by detecting HOCl. Upon reaction with HOCl, the emission intensity of the nanoprobe is significantly enhanced, allowing for susceptible and specific detection of neuroinflammation. They are designed to be BBB-permeable. They are also sensible and applicable in the diagnosis of lipopolysaccharide-induced neuroinflammation. These nanoprobes can be used to monitor neuroinflammation following a cerebral stroke.[41] Fig. 3 and Table 1 show the applications of UCNPs for biomolecular detection.

3.2 Cell imaging

Cell imaging is challenging when monitoring proteins or organelles inside cells because it is necessary to observe and analyze their structure, function, and dynamic processes without affecting cells' biological functions. Newly developed UCNP technology provides researchers with invaluable insight into the complex mechanisms inside cells, enhancing their understanding of biological processes and making it a promising basic research and clinical tool.[49] Therefore, it is crucial to evaluate their safety, biocompatibility, and toxicity comprehensively. For example, Bin Hu's group evaluated the cytotoxicity, uptake, and elimination process of UCNPs using HepG2 cells. They found that the cytotoxicity of UCNPs was caused by mitochondria-mediated generation of ROS and induction of apoptosis by oxidative stress, while being time- and dose-depen-

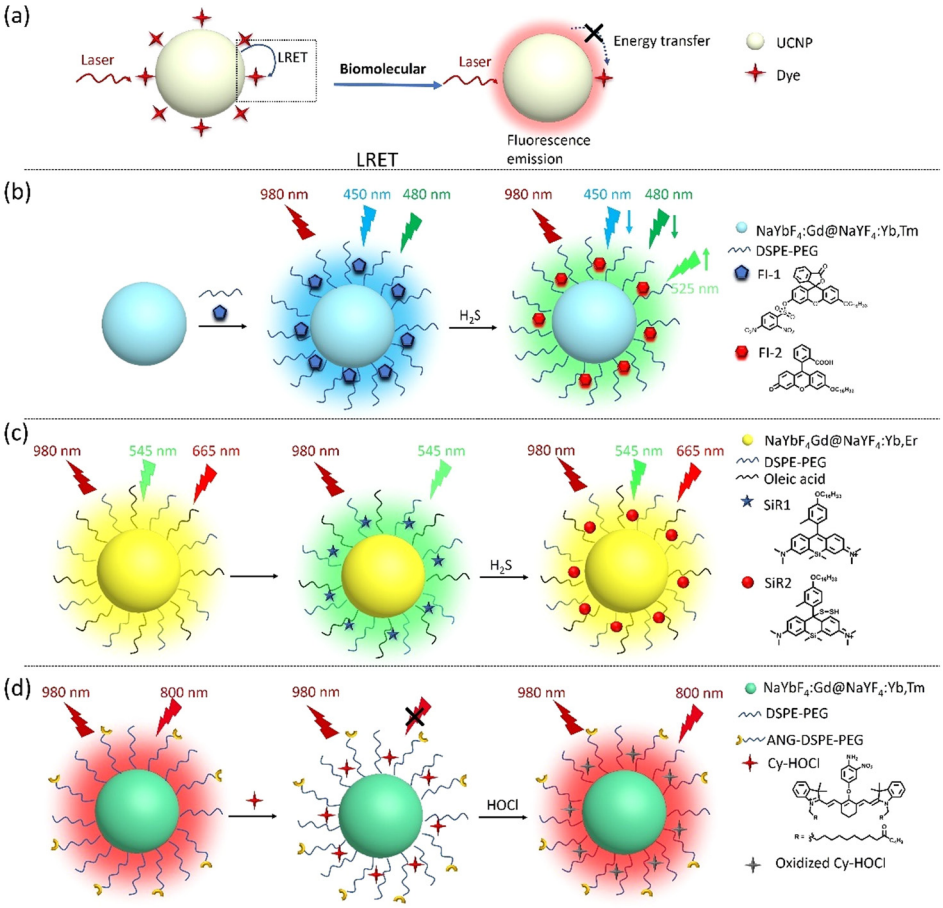

Fig. 3 (a) Schematic illustration of dye–UCNP probes based on the luminescence resonance energy transfer; (b) the construction of the FI-1–UCNP probe and its response mechanism to H_2S, and the change in the fluorescence signal is due to the transition of the organic dye FI-1 on the surface of UCNP to FI-2 after reacting with H_2S; (c) constructed SiR1–UCNP probe for the reversible detection of H_2S, and the fluorescence signal of $NaYbF_4Gd@NaYF_4$:Yb,Er at 665 nm was recovered after the reaction of SiR1 with H_2S; (d) illustration of the Cy-HOCl-UCNP probe for HOCl detection. The ANG peptide on the surface of the UCNPs determines their binding ability to brain endothelial cells, conferring their BBB permeability. Oxidation of Cy-HOCl destroys the spectral overlap between it and UCNPs, restoring UCL intensity at 800 nm.

Table 1 UCNP-based nanoprobe for biomolecular detection

Nanoprobe	UCNPs	Biomarker	Detection limit	Disease	Ref.
$NaGdF_4$:Yb^{3+},Er^{3+}@Ag-GOx	$NaGdF_4$:Yb,Er	Glucose	1.77 μM	High blood pressure, diabetes	16
Fl-1-UCNPs	$NaYbF_4$:Gd@$NaYF_4$:Yb,Tm	H_2S	0.741 μM	Arthritis, tumor/HCT116 cell	39
CMS-UCNPs@azo	$NaYF_4$@$NaYF_4$:Yb,Tm@$NaYF_4$:Yb, Er@$NaYF_4$	$^{\bullet}OH$	0.10 fM	Tumor/HeLa cells	40
CyH-UCNPs	$NaYbF_4$:Gd@$NaYF_4$:Yb/Tm	HOCl	0.9 μM	Cerebral stroke	41
$NaYF_4$:Yb,Er	$NaYF_4$:Yb,Er	Blood glucose	1.0 μM	Diabetes mellitus, hypoglycemia	43
$NaErF_4$:Tm@$NaGdF_4$:Yb	$NaErF_4$:Tm@$NaGdF_4$:Yb	Glucose, GSH in serum	0.03 μM, 0.075 μM	Diabetes, neurological diseases	44
SiR1-UCNPs	$NaYbF_4$:Gd@$NaYF_4$:Yb,Er	H_2S_n	0.486 μM	Liver injury	47
PAAO-UCNPs-EM1	$NaYF_4$:Yb,Tm@$NaYF_4$:Yb,Er	H_2S	0.121 μM	Tumor/HepG2 cells	48

dent.[50] Particularly, the cellular associations and heterogeneous interactions of UCNPs with human immune cells are critical. Z. Gerelkhuu *et al.* conducted a study using high-throughput single-cell techniques to investigate the complex interaction of Yb^{3+}/Er^{3+}-doped $NaYF_4$ UCNPs with human peripheral blood mononuclear cells (hPBMCs). Their study explored the affinity of different immune cells to UCNPs, describing the heterogeneous interactions between traditional

nanomaterials and the complex human immune system, facilitating the design and application of nanomaterials to ensure their safety in biomedical fields.[51]

By monitoring the direction of cell differentiation, early diagnosis of related diseases can be achieved (Fig. 4). For example, macrophages can be polarized into M1 macrophages with pro-inflammatory characteristics and M2 macrophages with anti-inflammatory characteristics. M1-type macrophages usually produce a series of cytokines and chemicals, such as ROS, which promote inflammatory responses, leading to tissue damage and plaque formation in atherosclerosis. M2 macrophages are in an anti-inflammatory and repair state. They suppress inflammation by secreting cytokines, such as interleukin-10 (IL-10), and promote tissue repair and healing. Feng Cao *et al.* developed a Gd-doped UCNP probe functionalized with a MARCO-targeting peptide. The macrophage receptor with a collagenous structure (MARCO) is a receptor expressed explicitly on the surface of pro-inflammatory macrophages (M1 macrophages), which plays a vital role in the occurrence and development of atherosclerotic plaques. Their novel UCNP emits green light under 980 nm laser excitation, enabling high-resolution visualization of M1 macrophages, while MRI provides detailed anatomical information about the plaque and surrounding tissue. Studying M1-type macrophage polarization in atherosclerotic plaques contributes to a better understanding of plaque progression and aids in developing new diagnostic and therapeutic strategies for atherosclerosis.[52]

Proteins are essential components of cells, and their unique characteristics determine biochemical reactions, tissue structure, and cell fate. Proteins are closely related to developmental regulation, homeostasis maintenance, and pathological progression. Albumin is a protein synthesized and secreted by hepatocytes in the liver. The differentiation status of liver organoids can be determined by monitoring albumin's expression and secretion levels. Guofeng Liu *et al.* developed a NIR-responsive nanoprobe called UCNPs-Ab-RBHA (UCAR) for quantitatively detecting albumin. This probe can distinguish the differentiation process of hepatobiliary duct-derived progenitor cells under different conditions, including their differentiation into organoids and hepatocytes. They presented

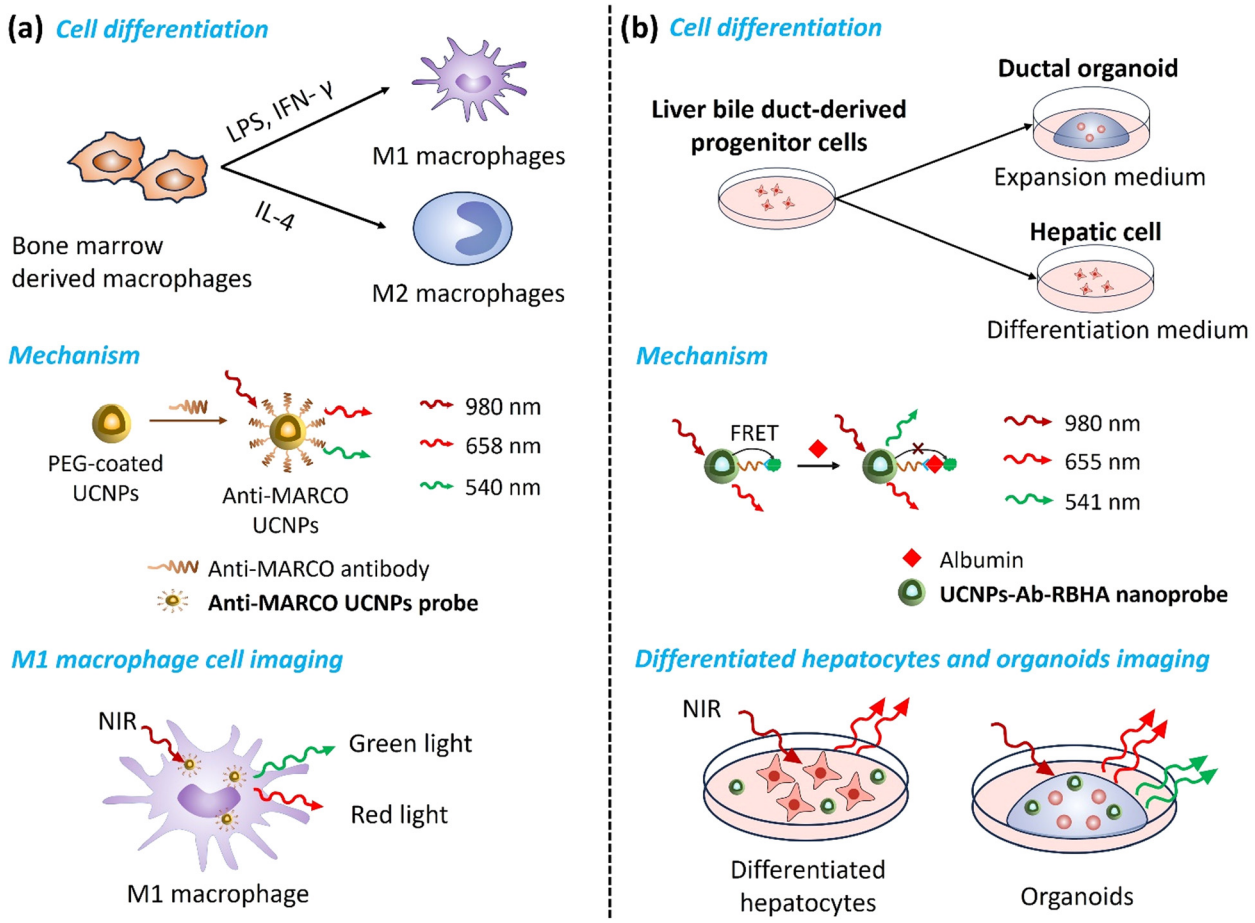

Fig. 4 Application of UCNPs in the early diagnosis of cell differentiation-related diseases. (a). Differentiation of bone marrow derived macrophages; anti-MARCO antibody modified UCNPs were used to target M1 macrophages; application of the anti-MARCO UCNP probe in M1 macrophage imaging for the diagnosis of atherosclerotic disease. (b) Differentiation of liver bile duct-derived progenitor cells; the response mechanism between the UCNPs-Ab-RBHA nanoprobe and organoids; UCNPs-Ab-RBHA nanoprobe recognition of differentiated hepatocytes and organoids imaging for research on hepatocyte-related diseases.

dynamic changes in proteins and cell functions in complex biological environments, which could be used to study hepatocyte cell development and the mechanisms involved in hepatocyte-related diseases.[18]

Neurological diseases are complex and involve abnormalities in the nerve cell structure, function, neurotransmitters, or chemical process and transmission. These can impact bodily functions such as movement, sensation, cognition, emotions, and other behavioral and physiological processes.[29] UCNP technology has been applied in neurotransmitter imaging,[53] neuroinflammation imaging,[54] and neural activity imaging.[55] By modifying the surface of UCNPs with targeting ligands, selective neurons can be tagged and tracked both *in vitro* and *in vivo*, allowing for a more comprehensive understanding of neurological diseases. Highly specialized UCNP technology can also be employed to investigate neuronal networks, their temporal and spatial activity characteristics, and the mechanisms of neuronal apoptosis. Understanding the mechanisms of internalization of nanoparticles in the central nervous system (CNS) and their effects on tissue morphology is important for developing new cell therapies and designing controlled nanoparticles for brain therapy.[31,56] Karolina Zajdel *et al.* evaluated the internalization mechanism, biodistribution, and neurotoxicity of UCNPs in rat hippocampal slices using an organotypic hippocampal slice culture (OHSC) model. They found that UCNPs are readily internalized by hippocampal cells and co-localize with specific organelles within neurons, astrocytes, endosomes, and lysosomes. UCNPs enter neurons through clathrin- and caveolae-mediated endocytosis. In addition, UCNPs are present in cells in early and late endosomes, lysosomes, and large autolysosomes. Higher concentrations of UCNPs may induce the autophagy process but do not affect the cellular response. These findings have important implications for understanding the interaction of nanomaterials with tissues and for developing therapeutic strategies at micro (cellular) and macro (brain) levels.[30]

Motor-proteins are a class of proteins that use adenosine triphosphate (ATP) energy to drive intracellular material transport by interacting with cytoskeletal proteins. Dynein-driven retrograde axonal transport moves intracellular cargos from axonal terminals to the soma. This process is essential for many physiological functions of neurons, including nutrient supply, molecular signaling, and organelle migration. Retrograde transport disorders are closely related to the development of neurodegenerative diseases. Xiao Zeng and colleagues used UCNPs to label motor proteins, observe and track the movement of individual motor proteins in real time, and visualize axonal transport processes. The feasibility of UCNP probes as potential tools for early screening of neurodegenerative diseases was verified by constructing a cell model of Rett syndrome. This high-resolution imaging and tracking approach contributes to a better understanding of intracellular transport mechanisms. It could also provide new targets and strategies for treating neurodegenerative diseases.[57] The applications of UCNP based nanoprobes for cell imaging are summarized in Table 2.

3.3 Cancer diagnosis

With the continuous progress of nanotechnology, UCNPs have emerged as a promising tool for tumor diagnosis due to their non-invasive, non-destructive, high sensitivity, super-resolution, and real-time imaging capabilities.[22] Synthetic UCNPs typically involve hydrophobic ligands, such as oleic acid (OA) or oleamide (OAm), which do not provide colloidal stability in aqueous media. To create water-soluble UCNPs, various methods can be used, but they may impact the individual particle brightness. For instance, these methods include ligand exchange to substitute the original hydrophobic ligands (3% quenching modified with $NOBF_4$, 84% quenching treated by HCl), coated through inorganic silica shell deposition (21% quenching modified with SiO_2, 71% quenching modified with $mSiO_2$), and amphiphilic polymer self-assembly *via* hydrophobic–hydrophobic interaction (8% quenching coated with DSPE-PEG).[58] There are also other limitations, such as cytotoxicity, lack of selectivity for specific tumor cells, limited imaging depth, and poor biocompatibility, that need to be considered as well.[59,60] Surface functionalization is necessary to overcome some of these challenges, and appropriate method selection will be more conducive to expanding its application.[61] Commonly used UCNP surface modification methods include polymer coating, biomacromolecule modification, metal ion doping, nucleotide modification, cell membrane coating, *etc*.[62–65] Surface modification of UCNPs can be tailored according to specific application requirements to achieve targeting modification, biocompatibility improvement, drug packaging, treatment, and other functions.[66,67]

Polyethylene glycol (PEG) is one of the most commonly used polymers for surface modification of UCNPs, which enhances the water dispersion, biocompatibility, and protein adsorption resistance of UCNPs. Additionally, the terminal group of PEG is easily modified to facilitate the functionalization of UCNPs.[68,69] Studies have shown that the length and graft density of the polymer coating can affect the physical, chemical, and biological properties of UCNPs. For instance, UCNPs with the longest polymer coating exhibited the highest tumor cell uptake potential and the longest cycle time at a lower graft density. However, when the graft density is too high, the polymer begins to detach from the UCNP surface, leading to decreased stability of UCNPs and instability in drug release.[62] PEG-modified UCNPs have been used for targeted imaging of liver cancer cells by attaching glycyrrhetinic acid (GA) to the PEG coating, which enhances the uptake of UCNPs by liver cancer cells and allows for precise imaging under NIR light excitation.[70] Additionally, glycosylated pegylated phospholipid (DSPE-PEG-Glu) modified UCNPs have been developed for detecting non-muscle invasive bladder cancer (NMIBC). The DSPE-PEG-Glu coating enhances UCNPs' targeting of glucose transport proteins (GLUTs), which are overexpressed in most cancer cells, thereby enhancing their aggregation in NMIBC.[63]

Cyclodextrins (CDs) are polysaccharides with amphiphilic structures that can also be used for surface modification of

Table 2 UCNP-based nanoprobe for cell imaging

Nanoprobe	UCNPs	Modification	Cell line	Ref.
PAA-UCNPs	$NaYF_4$:Er, Yb	Poly(acrylic acid)	HepG2 cell	50
UCNP@POEGMEA-*b*-PMEAP	$NaYF_4$:Er,Yb	Oligo ethylene glycol methyl ether acrylate (OEGMEA), block-bearing phosphate group (MAEP) diblock copolymer	hPBMCs	51
Anti-MARCO UCNPs	$NaGdF_4$:Yb, Er@$NaGdF_4$	PEG, polyclonal MARCO antibody	M1 macrophage	52
UCAR	$NaYF_4$:YbEr@$NaYF_4$	PEI, antibody, bovine serum albumin (BSA), rose bengal hexanoic acid (RBHA)	Hepatocyte organoids	18
$NaYF_4$:Yb,Tm,Gd	$NaYF_4$:Yb,Tm,Gd	Dipicrylamine, glutathione	HEK293 cells	55
$NaYF_4$:Yb,Er	$NaYF_4$:Yb,Er	SiO_2	OHSCs	30
$NaLuF_4$:Yb,Er	$NaLuF_4$:Yb,Er	SiO_2	Dorsal root ganglion neurons	57

UCNPs. CD modification is mainly used to enhance stability, increase the *in vivo* circulation time, improve the water solubility and biocompatibility of UCNPs, and reduce toxic side effects.[71] β-Galactosidase is a glycoside hydrolase, and its abnormal accumulation is closely related to the cellular aging process and various malignancies, such as primary ovarian cancer. Detao Jiang *et al.* developed a ratiometric nanoprobe based on LRET for β-galactosidase (β-gal) detection. α-CD on the surface of UCNPs was assembled with β-galactosidase modified pyranonitrile dye (DCM-β-gal) through hydrophobic interaction to form DCM-β-Gal-UCNP nanoprobes. After the addition of β-gal, the C–O bond of DCM-β-gal was broken by the enzymatic reaction, releasing DCM-β-Gal-OH with a strong intramolecular charge transfer (ICT). The maximum absorption of DCM-β-gal-UCNPs was redshifted from 440 nm to 543 nm, triggering the LRET process, and the near infrared UCL emission centered at 800 nm had no significant change. The UCL intensity ratio (UCL543 nm/UCL 800 nm) was used as the output signal to realize the highly sensitive detection of β-gal activity (low limit detection of 3.1×10^{-4} U mL^{-1}). In addition, DCM-β-gal-UCNPs can be effectively used to monitor β-gal in living cells and zebrafish tumor models.[19]

Researchers often use metal doping to enhance the luminescence efficiency of UCNPs and create nanoprobes for multimodal imaging.[26,72] Gold (Au) nanoparticles deposited on UCNPs (Au-UCNPs) have been widely used in CT, MRI fluorescence imaging (FL), and photoacoustic imaging (PAI) of tumors due to their excellent imaging ability and photothermal effect.[73] Au-UCNPs specifically target tumor cells through surface modification of targeted ligands to achieve highly accurate imaging and photothermal therapy (PTT). In PTT, Au-UCNPs absorb light energy under near-infrared light irradiation and converts it to heat by photothermal conversion. This locally generated heat can lead to thermal damage and cell death in tumor cells without affecting the surrounding healthy tissues.[74] Zeng's group developed a core–shell UCNP nanoplatform for NIR-II/MRI dual-modality imaging. The uniformly coated MnO_2 shell enhanced T_1-weighted MRI imaging and improved ROS release in the acidic tumor microenvironment.[75] Najim Akhtar *et al.* reported an upconversion nanoformulation UCNP@Tf-^{99m}Tc that enables dual-targeting (passive and active) and five-modality (infrared thermal imaging 'IRTI', UCL, MRI, SPECT, and CT) cancer imaging. The preparation is covalently conjugated to transferrin (Tf) to achieve active tumor targeting and evasion of the immune system. It also binds to technetium-99 m (^{99m}Tc) to achieve stability and radiolabeling efficiency. This nano-formulation has good biocompatibility with adequate renal clearance, which can be considered an effective 4T1 tumor imaging agent.[76]

The surface functionalization of UCNPs using cell membranes is one of the research hotspots. This method directly binds cell membranes to the surface of UCNPs, inheriting the unique surface physicochemical properties derived from cells. Compared with traditional preparation methods, cell membranes can endow UCNPs with a 'stealth function'. This function, which is a result of the cell membrane coating, effectively reduces the adsorption of non-specific proteins, prevents autoimmune attacks, and makes nanomaterials safer and more biocompatible.[64] Mengting Li and colleagues designed UCNPs coated with red blood cell (RBC) membranes (RBC-UCNPs) by binding 1,2-distearoyl-*sn-glycero*-3-phosphoethanola-mine-*N*-[folate(polyethyleneglycol)-2000] (DSPE-PEG-FA) to the cell membrane, enhancing the targeting ability of tumor cells. RBC-UCNPs have good biocompatibility *in vivo* with a prolonged circulation time (~36 h), which can be used for multimodal imaging (FL/PET/CT/MR) for 4T1 breast cancer.[65]

UCNPs have also been used for microRNA detection, as some miRNAs are overexpressed in various forms of tumors and have been widely used as biomarkers for cancer detection and prognosis. Li's group reported functionalized UCNPs with complementary capture template-aDNA3 complexes (CPT-aDNA3) and nucleic acid amplicons (BHQ1-tagged 8–17 DNAzyme) for miRNA detection (Fig. 5). The UCNPs act as energy donors, BHQ1 as an energy acceptor, resulting in the UCL quenching due to LRET, and CPT-aDNA3 as a DNA trap. When targeting miR-21, it binds with the CPT to release aDNA3, which can unlock 8–17 DNAzyme-BHQ1 to form the aDNA3-DNAzyme-BHQ1 duplex. The green UCL signal of UCNPs can be recovered after the "–rA–" site of this duplex is cleaved by Zn^{2+} ions, releasing BHQ1 from the DNAzyme terminal on the surface of UCNPs. Free aDNA3 triggers the next cycle to further amplify the signal of miR-21. The optimized UCNP nano-amplicon platform demonstrated the specificity

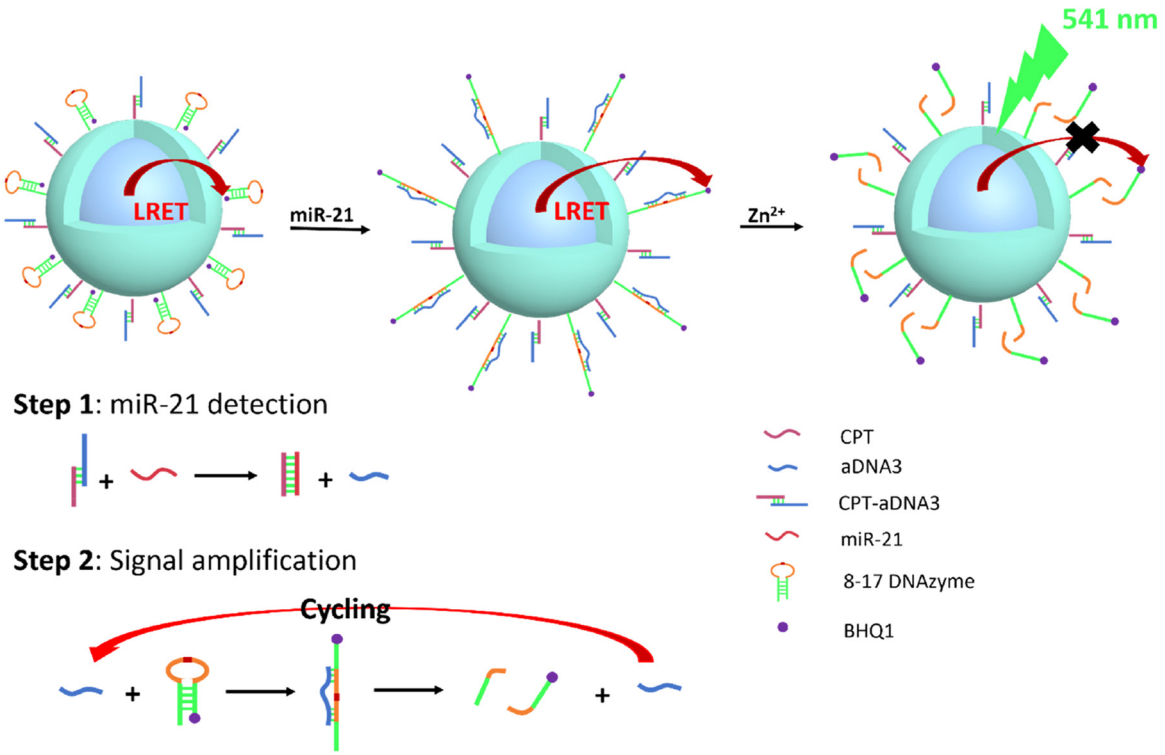

Fig. 5 Schematic representation of UCNP@DNAzyme-BHQ1/CPT-aDNA for miR-21 detection. Ultra-low detection limit (31 fM) test performed by signal amplification.

and sensitivity of microRNA (detection limit as low as 31 fM) *in vitro* and *in vivo*. This nano-amplicon enables *in situ* imaging of miRNA expression in living animals using fluorescence imaging technology and enables the detection of changes in miRNA expression levels after drug treatment.[77] The applications of UCNPs for tumor diagnosis are summarized in Table 3.

3.4 Deep tissue imaging

Several challenges must be addressed before UCNPs can be applied for *in vivo* imaging. First, the cytotoxicity of UCNP is affected by various factors such as size, shape, and surface modification. It is essential to optimize the size and surface chemistry of nanoprobes to minimize toxicity and enhance biocompatibility.[78] Second, reducing the non-specific binding of UCNPs to non-target tissues is necessary to achieve a relatively high signal-to-noise ratio. By ligand modification on their surface, UCNPs can contribute to site-specific aggregation, thereby reducing background signal interference.[79] Third, to overcome the limitations of fluorescence imaging in terms of tissue penetration, UCNPs shall be designed as a NIR fluorescent probe. NIR light has a longer wavelength with lower absorption and scattering in biological tissues and hence, it penetrates deeper and remains less perturbed in the biological transparent window (650–1350 nm).[80] Thus, non-invasive *in vivo* imaging can be achieved to improve the depth and resolution of imaging.[11]

In the following section, we discuss the application of UCNPs in vascular imaging, CNS disease diagnosis and treatment, and multimodal imaging (Fig. 6).

Table 3 UCNP-based nanoprobe for tumor diagnosis

UCNP	Modification	Targeting ligand	Imaging method	Tumor/tumor cells	Ref.
UCNP@P80-1	PPEGMEM	—	UCL	MCF-7 cells	62
GA-CSS UCNPs	PEG	GA	UCL/MR	HepG2 cells	70
UCNP-G100	DSPE-PEG-Glu	DSPE-PEG-Glu	UCL	Non-muscle invasive bladder cancer	63
DCM-β-gal-UCNPs	CD	DCM-β-gal	UCL	Ovarian cancer	19
Au-UCNPs-DSPE-PEG2K	PEG	—	PA/MRI/CT	HeLa cell	74
UCNP@Tf-^{99m}Tc	Tf	Tf	IRTI/UCL/MRI/SPECT//CT	4T1 cell	76
RBC-UCNPs	RBC membranes	DSPE-PEG-FA	FL/PET/CT/MR	4T1 breast cancer	65
UCNP@DNAzyme-BHQ1/CPT-aDNA	—	CPT-aDNA3	UPL	HeLa cell	77

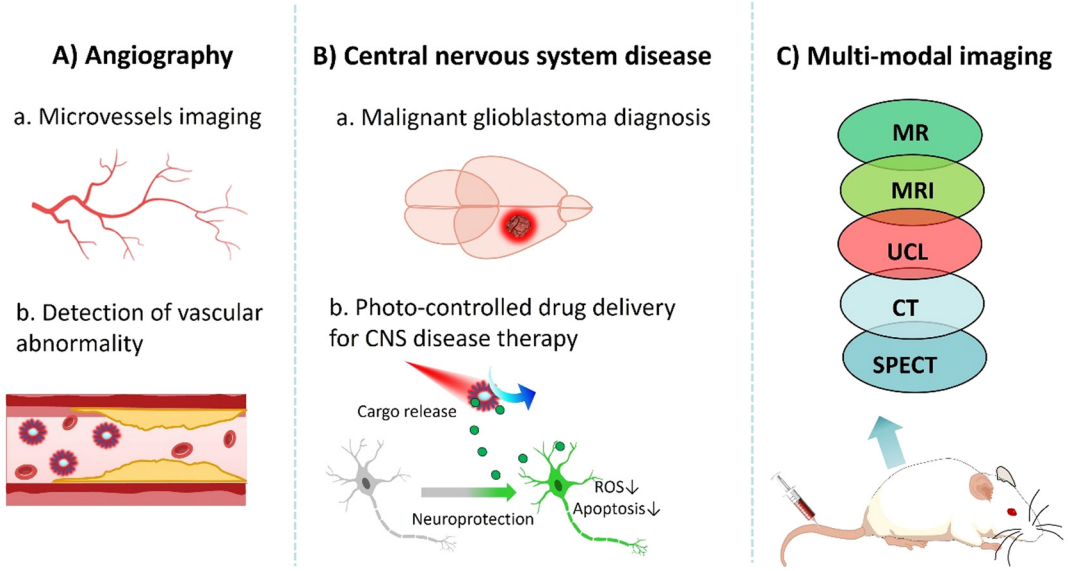

Fig. 6 Schematic representation of UCNPs for *in vivo* imaging. (A) Angiography: (a) neovascularization imaging and (b) vascular inflammation diagnosis; (B) central nervous system (CNS) diseases: (a) malignant glioblastoma diagnosis and (b) photo-controlled drug delivery for CNS disease therapy; and (C) *in vivo* multimodal imaging.

UCNPs with high emission light intensity and a low background signal can provide high-contrast images of blood vessels and detect the presence and formation of micro-vessels and abnormal vasculatures. Angiogenesis could be associated with some diseases, like vascular inflammation. Under the stimulation of an inflammatory response, vascular endothelial cells release proangiogenic factors, such as vascular endothelial growth factor (VEGF) and basic fiber growth factor (bFGF), which promote the proliferation and migration of endothelial cells, thereby promoting the formation of new blood vessels.[81] Tumor cells also release proangiogenic factors that stimulate the formation of new vascular networks in their surrounding tissues. Such formation of neovascularization in relation to the presence of tumors provides sufficient oxygen and nutrients for tumor cells. It also plays an important role in tumor growth and metastasis. Therefore, targeting neovascularization has become increasingly one of the critical characteristics for diagnosis and treatment monitoring.[82] As a consequence, the surface functionalization of UCNPs is required to ensure the chemical and colloidal stability of UCNPs in a buffer system, prolonged circulation time, deep tissue penetration, and low nonspecific adsorption by/from/to blood proteins, with great sensitivity and selectivity. Shane Plunkett and co-workers used a Janus-type dendrimer as a surface ligand with multiple carboxyl groups attached to UCNPs on one "surface" and polyethylene glycol (PEG) on the other "surface" to confer water solubility to UCNPs. UCNP/Janus-dendritic molecules have shown excellent function as vascular markers. They were successfully used to map the depth resolution of a single capillary in the mouse brain at a remarkable depth of 1000 μm under continuous wave excitation with a power of no more than 20 mW. Compared to conventional two-photon microscopy using red fluorescent dyes such as Alexa 680, the required time-averaged power is significantly reduced, typically around 100 mW. This optimization allowed high-quality image acquisition at a lower power level while reducing the potential risk of damage to the sample. Extraordinary high-resolution images were obtained even at high scanning speeds.[83] Polina A. Demina *et al.* used carboxylic acid (CA) to coat UCNPs, thus obtaining nanoparticles with "invisible" properties. CA is a highly hydrophilic homopolymeric compound composed of sialic acid residues, with no known toxicity and immune reactions, which also has the property of low nonspecific blood protein adsorption. This allows the CA-coated UCNPs to have a long circulation time *in vivo.* They can also safely accumulate during microvascular remodeling at the inflammatory site. By using CA modified UCNPs, inflammation imaging in systemic mode can be achieved, and local visualization of blood vessels *in vivo* can be used to diagnose and monitor inflammatory disease treatment.[84]

Upconversion nanomaterials can be implanted in deeper tissue, which can play an essential role in diagnosing and treating central nervous system diseases.[85] Malignant glioblastoma is one of the most common primary brain tumors. Its occult nature and location (confined within the skull) make early diagnosis difficult. Due to its highly aggressive nature and heterogeneity, malignant glioblastoma can deeply invade the adjacent brain parenchyma, resulting in further difficulties in distinguishing the boundary of the tumor from healthy tissue. Furthermore, even with surgical resection, recurrence is inevitable due to residual glioblastoma cells within the neighboring brain parenchyma. The study by Miaomiao Cheng *et al.* used a pegylated functionalized UCNP ($KMnF_3$:Yb,Er) nanoprobe coupled with biotin to achieve precise imaging of glio-

Table 4 UCNP-based nanoprobe for *in vivo* imaging

Nanoprobe	UCNP	Modification	Imaging method	Disease	Ref.
$NaYF_4$:Er,Yb	$NaYF_4$:Er,Yb	Janus-dendrimers	UCL	Brain vasculature	83
UCNP-CA	$NaYF_4$:Yb,Tm@$NaYF_4$	Colominic acid	UCL	Inflammation	84
PDA@UCNPs	$NaGdF_4$:Er,Yb	PEG	UCL	Mouse melanoma	85
Biotin/PEG-UCNPs	$KMnF_3$:Yb,Er	Biotin/PEG	MR/UCL	Glioblastomas	86
Lf-UZSP	$NaYF_4$:Yb,Tm@$NaYF_4$	Polyvinylpyrrolidone, zeolitic imidazolate framework-8	UCL	Parkinson's disease	54
UCNP-PS	$NaGdF_4$:Yb,Er	Transferrin protein	MRI/UCL	4T1 breast cancer	87
$ZnAl_2O_4$:$^{171/169}$Er	$ZnAl_2O_4$:$^{171/169}$Er	—	SPECT/UCL	Mouse melanoma	88
Gd_2O_2S:Yb,Tm	Gd_2O_2S:Yb,Tm	—	CT/MR/UCL	—	89

blastoma by targeting the sodium-dependent multivitamin transporter (SMVT) overexpressed on the surface of cancer cells. The $KMnF_3$ master lattice endows the nanoprobe with MR imaging capabilities. Biotin/PEG-UCNPs have good biocompatibility and low *in vivo* toxicity, making them promising candidates as MR/UCL imaging agents for the invasion area of glioblastoma to potentially guide a much better, near complete surgical resection. This translational research trend has the potential to become the clinically acceptable norm to improve the accuracy of early diagnosis and surgical resection of glioblastoma.[86]

Parkinson's disease (PD) is a neurodegenerative disease that leads to disability in the elderly, though its etiology and pathogenesis are not fully understood. It is generally believed that oxidative stress and neuroinflammation play important roles in the development of PD. Non-invasive delivery of drugs for the treatment of PD needs to cross the BBB, reduce oxidative stress, and inhibit neuroinflammation and apoptosis. Photo-controlled drug delivery uses photosensitive molecules or nanomaterials to trigger the release or activation of drugs when they are irradiated with light of a specific wavelength or intensity. Therefore, they could realize the spatiotemporal regulation of drug release and improve the accuracy and effect of treatment. The application of the UCNP system in photo-controlled drug delivery for PD treatment has shown excellent properties due to the strong tissue penetration of excited NIR light, controllable emission light, small size, and desired surface modification. Binbin Hu *et al.* constructed a nanosystem using UCNPs as carriers for photo-controlled delivery of *S*-nitroso-*N*-acetyl-DL-penicillamine (SNAP) and paeoniflorin (Pae). By modifying lactoferrin (Lf) on the surface of UCNPs, which could combine with the highly expressed lactoferrin receptor on the surface of cerebrovascular endothelial cells, UCNPs can cross the BBB and accumulate in the microenvironment of PD brain tissue. Under NIR light irradiation, UCNPs can convert NIR light to UV light, stimulating the release of NO from SNAP and promoting the release of Pae from the nanocarrier. The released NO and Pae can jointly remove ROS from the microenvironment, inhibit neuroinflammation, reduce the loss of dopaminergic (DA) neurons in the substantia nigra and striatum, and improve motor behavioral related symptoms in patients suffering from PD.[54]

Combining UCL and nuclear imaging to construct multimodal imaging is one of the innovative ways to address the poor tissue penetration of fluorescence imaging.[87,88] Mauricot's group reported a new type of UCNP, Gd_2O_2S:Yb^{3+}/Tm^{3+}, which exhibits strong fluorescence emission at 802 nm when excited using a 980 nm laser. This enables them to reach deeper structures of the CNS and reduce or eliminate the effect of autofluorescence. Consequently, a higher signal-to-noise ratio and deeper tissue penetration are possible. In addition, a large amount of notably paramagnetic Gd in these UCNPs also brings about interesting contrast properties in MRI and CT, which can be exploited in multimodal *in vivo* imaging. With a customized imaging system, the fluorescence signals of UCNPs can be detected in different tissues such as skin, muscle, kidney, liver, and brain, and at different depths for a relatively longer time after *in situ* injection. Results show that the nanoparticles are suitable for deep tissue imaging, and high resolution and high sensitivity information can be obtained through multimodal imaging.[89] Examples of UCNPs for deep *in vivo* imaging are summarized in Table 4.

The programmable light emission of UCNPs at a specific wavelength has been considered a powerful tool to facilitate optogenetic applications, enabling precise temporal and spatial manipulation of neuronal activity.[57,90,91] In many recent studies, UCNPs implanted near opsin-expressing neurons were used to convert NIR illumination into a spectrum of visible emissions, effectively regulating ChR light-gated ion channels. Today, implementing various forms of UCNPs in biological systems is becoming a valuable research tool for scientists and researchers studying neurodegenerative diseases.[31,56,92,93]

4. Discussion

UCNPs have emerged as versatile tools with immense potential for revolutionizing biomedical imaging applications. Their ability to convert near-infrared light into visible and ultraviolet emissions makes them highly attractive for various biological imaging techniques, including *in vitro* and *in vivo* molecular sensing, cellular tracking, tumor diagnosis, and tissue imaging.

Looking forward, significant advances are anticipated in UCNP research. Responsively, the surface of UCNPs can be modified with biological macromolecules, fluorescent markers, and targeted molecules to achieve binding to the targeted molecules and improve the sensitivities, specificities, and resolution of imaging. Highly sensitive off–on nanoprobes were synthesized using the LRET mechanism by introducing organic dyes as energy acceptors. Surface modification could also increase the intracellular stability and uptake performance of UCNPs, thereby improving their application potential in cellular imaging. In tumor diagnosis, UCNPs can achieve high specific recognition in tumor cell imaging by modifying their targeted ligands. This application can improve the sensitivity and resolution of tumor imaging and is expected to become a valuable tool for tumor diagnosis and treatment in the near future. In addition, UCNPs can also be used for neuronal imaging and diagnosis in the CNS. Since crossing the BBB remains a significant challenge for most drugs, developing and implementing safe and effective medical treatments for CNS diseases continues to face substantial obstacles. The introduction of the concept of various forms and constructs of UCNPs could help overcome some of these obstacles. UCNPs can be integrated into multimodal imaging to obtain precise imaging signals and enhance the accuracy of diagnostics in CNS pathologies and even treatments *via* neuromodulation.

Although utilizing UCNPs in biological systems brings about many advantages for diagnosis, imaging, and treatments, other restrictive and critical disadvantages must also be considered and overcome. These limitations include potential low luminescence efficiency due to radiation loss during energy transfer and the use of high energy lasers, which may cause photodamage or have photothermal effects on biological tissues, as well as concerns regarding biocompatibility, cytotoxicity, and stability that still need to be investigated and improved. Additionally, there are challenges related to the time and complexity of their preparation, limitations in their mass production, cost, and large-scale applications. Each one of these limitations and challenges would be an opportunity to improve and optimize the application of UCNPs in biological systems. The synthesis of UCNPs with high quantum yields faces essential challenges, including maintaining high quantum yields in physiological environments, extreme pH, abnormal salinity, and abnormal oxidation or reduction conditions. In an aqueous solution, the oxygen and hydrogen ions in water molecules may transfer non-radiative energy to the excited state levels of lanthanide ions, resulting in attenuation or quenching of UCNP fluorescence. This phenomenon limits the quantum yield of UCNPs in aqueous solutions, thus limiting their potential for clinical applications. In addition, the upconversion efficiency of UCNPs is also affected by many factors, such as lanthanide selection, doping ratio, UCNP size, surface modification, and so on. A passivation shell is a crucial choice to enhance the fluorescence intensity of UCNPs, but inappropriate surface passivation can lead to a reduction or even loss of luminous efficiency. Moreover, LRET-based small molecule testing requires controlling the passivation shell's thickness, as the detection accuracy depends on the distance between the small molecule and the lanthanide ions in UCNPs. A comprehensive evaluation of the biocompatibility of UCNP nanoprobes is essential, especially for their use in clinical applications. While numerous studies have demonstrated the safety of UCNPs for bioimaging, their long-term biosafety remains to be determined. For instance, in studies on UCNPs for diagnosing central nervous system diseases, UCNPs are injected intravenously and travel through the blood circulation to brain vessels and then cross the blood–brain barrier into the brain. However, little has been reported about how the brain clears it after the work is done and whether it causes latent harm. This underscores the need for further research to ensure the safe use of UCNPs in clinical applications.

Despite these challenges, potential breakthroughs are on the horizon. Future research efforts may focus on integrating UCNPs with advanced imaging technologies such as photoacoustic imaging and magnetic resonance imaging, thereby expanding their utility in multimodal imaging approaches. Moreover, the development of UCNP-based theranostic platforms holds promise for simultaneous imaging and targeted therapy, paving the way for personalized medicine applications. In addition, the applications of UCNPs are poised to extend beyond traditional imaging. They are expected to play pivotal roles in precise surgical navigation, real-time monitoring of therapeutic responses, and even in the emerging field of optogenetics, where light-sensitive UCNPs can enable controlled cellular activities.

Author contributions

Writing – original draft preparation, Hengde Li and Haitao Liu; review and editing, Ka-Leung Wong and Angelo H. All; supervision, Angelo H. All; funding acquisition, Angelo H. All. All authors have read and given approval to the final version of the manuscript.

Data availability

No primary research results, software or code have been included and no new data were generated or analysed as part of this review.

Conflicts of interest

There are no conflicts to declare.

Acknowledgements

This study was supported by the grant sponsored by the 2021-24 Hong Kong Research Grant Council General Research Fund (GRF) # 12100121 (PI: Angelo All), Hong Kong SAR, China, and Initiation Grant Faculty Niche Research Areas Fund RC-FNRA-IG/20-21/SCI/02 (PI: Angelo All), Hong Kong SAR, China.

References

1 L. Liang, X. Qin, K. Zheng and X. Liu, *Acc. Chem. Res.*, 2018, **52**, 228–236.
2 K. Malhotra, D. Hrovat, B. Kumar, G. Qu, J. V. Houten, R. Ahmed, P. A. E. Piunno, P. T. Gunning and U. J. Krull, *ACS Appl. Mater. Interfaces*, 2023, **15**, 2499–2528.
3 P. K. Chintamaneni, D. Nagasen, K. C. Babu, A. Mourya, J. Madan, D. A. Srinivasarao, R. K. Ramachandra, P. M. Santhoshi and S. K. S. S. Pindiprolu, *J. Controlled Release*, 2022, **352**, 652–672.
4 K. Du, J. Feng, X. Gao and H. Zhang, *Light: Sci. Appl.*, 2022, **11**, 222.
5 N. J. J. Johnson, S. He, S. Diao, E. M. Chan, H. Dai and A. Almutairi, *J. Am. Chem. Soc.*, 2017, **139**, 3275–3282.
6 S. Wen, J. Zhou, K. Zheng, A. Bednarkiewicz, X. Liu and D. Jin, *Nat. Commun.*, 2018, **9**, 2415.
7 B. Grauel, C. Würth, C. Homann, L. Krukewitt, E. Andresen, J. Roik, S. Recknagel, M. Haase and U. Resch-Genger, *Nano Res.*, 2022, **15**, 2362–2373.
8 L. Liang, D. B. L. Teh, N.-D. Dinh, W. Chen, Q. Chen, Y. Wu, S. Chowdhury, A. Yamanaka, T. C. Sum and C.-H. Chen, *Nat. Commun.*, 2019, **10**, 1391.
9 M. Wang, C. Mi, W. Wang, C. Liu, Y. Wu, Z. Xu, C. Mao and S. Xu, *ACS Nano*, 2009, **3**, 1580–1586.
10 G. Bao, S. Wen, W. Wang, J. Zhou, S. Zha, Y. Liu, K.-L. Wong and D. Jin, *Nano Lett.*, 2021, **21**, 9862–9868.
11 L. Liang, X. Xie, D. T. B. Loong, A. H. All, L. Huang and X. Liu, *Chem. – Eur. J.*, 2016, **22**, 10801–10807.
12 A. A. Ansari, A. K. Parchur, N. D. Thorat and G. Chen, *Coord. Chem. Rev.*, 2021, **440**, 213971.
13 A. Selva Sharma, M. Marimuthu, A. W. Varghese, J. Wu, J. Xu, L. Xiaofeng, S. Devaraj, Y. Lan, H. Li and Q. Chen, *Crit. Rev. Food Sci. Nutr.*, 2022, **23**, 1–31.
14 J. Sobhanan, J. V. Rival, A. Anas, E. S. Shibu, Y. Takano and V. Biju, *Adv. Drug Delivery Rev.*, 2023, **197**, 114830.
15 S. Yan, Z. Luo, Z. Li, Y. Wang, J. Tao, C. Gong and X. Liu, *Angew. Chem.*, 2020, **132**, 17484–17495.
16 S. Zha, H. Li, G.-L. Law, K.-L. Wong and A. H. All, *Mater. Des.*, 2023, **227**, 111800–111809.
17 R. Xu, H. Cao, D. Lin, B. Yu and J. Qu, *Cell Rep. Phys. Sci.*, 2022, **3**, 1–15.
18 G. Liu, J. Wei, X. Li, M. Tian, Z. Wang, C. Shen, W. Sun, C. Li, X. Li and E. Lv, *Adv. Sci.*, 2022, **9**, 2202505.
19 D. Jiang, Q. Tan, Y. Shen, M. Ye, J. Li and Y. Zhou, *Spectrochim. Acta, Part A*, 2023, **292**, 122411.
20 A. Hlaváček, Z. Farka, M. J. Mickert, U. Kostiv, J. C. Brandmeier, D. Horák, P. Skládal, F. Foret and H. H. Gorris, *Nat. Protoc.*, 2022, **17**, 1028–1072.
21 G. Liang, H. Wang, H. Shi, H. Wang, M. Zhu, A. Jing, J. Li and G. Li, *J. Nanobiotechnol.*, 2020, **18**, 1–22.
22 R. Pu, Q. Zhan, X. Peng, S. Liu, X. Guo, L. Liang, X. Qin, Z. W. Zhao and X. Liu, *Nat. Commun.*, 2022, **13**, 6636.
23 J. Wang, P. Shangguan, M. Lin, L. Fu, Y. Liu, L. Han, S. Chen, X. Wang, M. Lu and Z. Luo, *ACS Nano*, 2023, **17**, 16840–16853.
24 J. Du, T. Jia, J. Zhang and G. Chen, *Adv. Opt. Mater.*, 2023, **11**, 2202122.
25 G. Kuang, H. Lu, S. He, H. Xiong, J. Yu, Q. Zhang and Y. Huang, *Adv. Healthcare Mater.*, 2021, **10**, e2100938.
26 T. Zhou, S. Zhang, L. Zhang, T. Jiang, H. Wang, L. Huang, H. Wu, Z. Fan and S. Jing, *Acta Biomater.*, 2023, **164**, 496–510.
27 L. Liang, C. Wang, J. Chen, Q. Wang and X. Liu, *Nat. Photonics*, 2022, **16**, 712–717.
28 Z. Yi, Z. Luo, N. D. Barth, X. Meng, H. Liu, W. Bu, A. All, M. Vendrell and X. Liu, *Adv. Mater.*, 2019, **31**, e1901851.
29 Y. Liu, Z. Yi, Y. Yao, B. Guo and X. Liu, *Acc. Mater. Res.*, 2022, **3**, 247–258.
30 K. Zajdel, J. Janowska, M. Frontczak-Baniewicz, J. Sypecka and B. Sikora, *Int. J. Mol. Sci.*, 2023, **24**, 1122.
31 S. Chen, A. Z. Weitemier, X. Zeng, L. He, X. Wang, Y. Tao, A. J. Y. Huang, Y. Hashimotodani, M. Kano and H. Iwasaki, *Science*, 2018, **359**, 679–684.
32 E. M. Mettenbrink, W. Yang and S. Wilhelm, *Adv. Photonics Res.*, 2022, **3**, 2200098.
33 F. Auzel, *C. R. Acad. Sci. Paris*, 1966, **263**, 819–821.
34 C. Duan, L. Liang, L. Li, R. Zhang and Z. P. Xu, *J. Mater. Chem. B*, 2018, **6**, 192–209.
35 K. Lingeshwar Reddy, R. Balaji, A. Kumar and V. Krishnan, *Small*, 2018, **14**, 1801304.
36 M. Zhang, P. Huang, W. Zheng, X. Song, X. Shang, W. Zhang, D. Yang, X. Yi and X. Chen, *Nano Lett.*, 2023, **23**, 8576–8584.
37 J. Wang, T. Sheng, X. Zhu, Q. Li, Y. Wu, J. Zhang, J. Liu and Y. Zhang, *Mater. Chem. Front.*, 2021, **5**, 1743–1770.
38 J. Peng, A. Samanta, X. Zeng, S. Han, L. Wang, D. Su, D. T. B. Loong, N. Y. Kang, S. J. Park and A. H. All, *Angew. Chem., Int. Ed.*, 2017, **56**, 4165–4169.
39 M. Zuo, Q. Duan, C. Li, J. Ge, Q. Wang, Z. Li and Z. Liu, *Anal. Chem.*, 2021, **93**, 5635–5643.
40 X. Song, J. Zhang, Z. Yue, Z. Wang, Z. Liu and S. Zhang, *Anal. Chem.*, 2017, **89**, 11021–11026.
41 M. Zhang, M. Zuo, C. Wang, Z. Li, Q. Cheng, J. Huang, Z. Wang and Z. Liu, *Anal. Chem.*, 2020, **92**, 5569–5576.
42 Y. Shuai, N. Li, Y. Zhang, Q. Bao, T. Wei, T. Yang, Q. Cheng, W. Wang, B. Hu and C. Mao, *Biosens. Bioelectron.*, 2024, **258**, 116335.
43 X. Chen, Z. Yang, Q. Chen and Y. Zhang, *Front. Bioeng. Biotechnol.*, 2023, **11**, 1168086.
44 T. Zhao, D. Wu, X. Zhang and H. Lyu, *Anal. Chim. Acta*, 2024, **1295**, 342323.
45 Z. Zhao, W. Guo, C. Xu, Q. Wang, C. Mao and M. Wan, *Chem. Eng. J.*, 2023, **452**, 139089.
46 U. Głowacka, T. Brzozowski and M. Magierowski, *Biomolecules*, 2020, **10**, 445.
47 Q. Duan, Y. He, W. Bi, T. Liang, Z. Liu and Z. Li, *Anal. Chem.*, 2022, **94**, 8792–8801.
48 M. Cui, H. Li, X. Ren, L. Xia, D. Deng, Y. Gu, D. Li and P. Wang, *Nanoscale*, 2020, **12**, 17517–17529.
49 Z. Zhang, Y. Chen and Y. Zhang, *Small*, 2022, **18**, 2103241.
50 C. Wang, M. He, B. Chen and B. Hu, *Ecotoxicol. Environ. Saf.*, 2020, **203**, 110951.

51 Z. Gerelkhuu, H. Perumalsamy, M. Maddahfar, D. Jin, J. Song and T. H. Yoon, *Environ. Sci.: Nano*, 2023, **10**, 824–833.
52 Y. Wang, Y. Zhang, Z. Wang, J. Zhang, R. R. Qiao, M. Xu, N. Yang, L. Gao, H. Qiao and M. Gao, *Biomaterials*, 2019, **219**, 119378.
53 S. Abbasi-Moayed, A. Bigdeli and M. R. Hormozi-Nezhad, *ACS Appl. Mater. Interfaces*, 2020, **12**, 52976–52982.
54 B. Hu, H. Fang, Z. Huang, W. Huang, L. Huang, H. Liu, F. Lv, W. Huang and X. Wang, *Chem. Eng. J.*, 2023, **465**, 142959.
55 J. Liu, R. Zhang, C. Shang, Y. Zhang, Y. Feng, L. Pan, B. Xu, T. Hyeon, W. Bu and J. Shi, *J. Am. Chem. Soc.*, 2020, **142**, 7858–7867.
56 A. H. All, X. Zeng, D. B. L. Teh, Z. Yi, A. Prasad, T. Ishizuka, N. Thakor, Y. Hiromu and X. Liu, *Adv. Mater.*, 2019, **31**, 1803474.
57 X. Zeng, S. Chen, A. Weitemier, S. Han, A. Blasiak, A. Prasad, K. Zheng, Z. Yi, B. Luo and I. H. Yang, *Angew. Chem., Int. Ed.*, 2019, **58**, 9262–9268.
58 H. Ling, D. Guan, R. Wen, J. Hu, Y. Zhang, F. Zhao, Y. Zhang and Q. Liu, *Small*, 2024, **20**, 2309035.
59 S. Zha, Y. H. Fung, H.-F. Chau, J. Lin, J. Wang, L. S. Chan, G. Zhu, H. L. Lung and K.-L. Wong, *Nanoscale*, 2018, **10**, 15632–15640.
60 S. Zha, H. F. Chau, W. Y. Chau, L. S. Chan, J. Lin, K. W. Lo, W. C. S. Cho, Y. L. Yip, S. W. Tsao and P. J. Farrell, *Adv. Sci.*, 2021, **8**, 2002919.
61 L. Arellano, R. Martínez, A. Pardo, I. Diez, B. Velasco, A. Moreda-Piñeiro, P. Bermejo-Barrera, S. Barbosa and P. Taboada, *J. Colloid Interface Sci.*, 2024, **668**, 575–586.
62 L. Zhang, C. Chen, S. S. Tay, S. Wen, C. Cao, M. Biro, D. Jin and M. H. Stenzel, *ACS Appl. Mater. Interfaces*, 2021, **13**, 16142–16154.
63 B. Sun, S. S. Mullapudi, Y. Zhang and K. G. Neoh, *Microchim. Acta*, 2022, **189**, 349.
64 D. Lu, J. R. Retama, R. Marin, M. I. Marqués, O. G. Calderón, S. Melle, P. Haro-González and D. Jaque, *Small*, 2022, **18**, 2202452.
65 M. Li, H. Fang, Q. Liu, Y. Gai, L. Yuan, S. Wang, H. Li, Y. Hou, M. Gao and X. Lan, *Biomater. Sci.*, 2020, **8**, 1802–1814.
66 Z. Luo, Z. Yi and X. Liu, *Acc. Chem. Res.*, 2023, **56**, 425–439.
67 Z. Luan, X. Ma, Q. Zhao, A. Yang and J. Li, *Chem. Eng. J.*, 2024, **488**, 150611.
68 K. Shwetabh, A. Banerjee, R. Poddar and K. Kumar, *J. Alloys Compd.*, 2024, **980**, 173493.
69 O. Dukhno, S. Ghosh, V. Greiner, S. Bou, J. Godet, V. Muhr, M. Buchner, T. Hirsch, Y. Mély and F. Przybilla, *ACS Appl. Mater. Interfaces*, 2024, **16**, 11217–11227.
70 J. E. Choi, H.-K. Kim, Y. Kim, G. Kim, T. S. Lee, S. Kim, D. Kim and H. S. Jang, *Mater. Des.*, 2020, **195**, 108941.
71 S. Hu, L. Huang, L. Zhou, T. Wu, S. Zhao and L. Zhang, *Anal. Chem.*, 2023, **95**, 3830–3839.
72 Y. Li and Y. Li, *Talanta*, 2022, **248**, 123641.
73 W. Zhang, Z. Liao, X. Meng, A. E. A. Niwaer, H. Wang, X. Li, D. Liu and F. Zuo, *Appl. Surf. Sci.*, 2020, **527**, 146821.
74 W. Zhang, Y. Zang, Y. Lu, J. Han, Q. Xiong and J. Xiong, *Int. J. Mol. Sci.*, 2022, **23**, 1382.
75 Y. Li, L. Du, F. Li, Z. Deng and S. Zeng, *ACS Appl. Mater. Interfaces*, 2022, **14**, 14944–14952.
76 N. Akhtar, P. Wu, C. Chen, W. Chang, R. S. Liu, C. T. Wu, A. Girigoswami and S. Chattopadhyay, *ACS Appl. Nano Mater.*, 2022, **5**, 7051–7062.
77 Y. Zhang, D. Luo, Y. Zhang, Q. Zhang, Q. Ji, S. Zhou, S. Huang, L. Li, F. Lu and W. Yao, *Chem. Eng. J.*, 2023, **454**, 140489.
78 L. M. Urdzíková, D. Mareková, T. Vasylyshyn, P. Matouš, V. Patsula, V. Oleksa, O. Shapoval, M. Vosmanská, D. Liebl and A. Benda, *Int. J. Mol. Sci.*, 2024, **25**, 5294.
79 S. Zhang, P. Liu, L. Li, Z. Liu, X. Qian, X. Jiang, W. Sun, L. Wang and E. U. Akkaya, *ACS Appl. Mater. Interfaces*, 2023, **15**, 40280–40291.
80 G. J. Richards, A. Cador, S. Yamada, A. Middleton, W. A. Webre, J. Labuta, P. A. Karr, K. Ariga, F. d'Souza and S. Kahlal, *J. Am. Chem. Soc.*, 2019, **141**, 19570–19574.
81 Y. Dun, H. Hu, F. Liu, Y. Shao, D. He, L. Zhang and J. Shen, *Biomed. Pharmacother.*, 2023, **162**, 114654.
82 Q. Wang, T. Liang, J. Wu, Z. Li and Z. Liu, *ACS Appl. Mater. Interfaces*, 2021, **13**, 29303–29312.
83 S. Plunkett, M. El Khatib, İ. Şencan, J. E. Porter, A. T. N. Kumar, J. E. Collins, S. Sakadžić and S. A. Vinogradov, *Nanoscale*, 2020, **12**, 2657–2672.
84 P. A. Demina, N. V. Sholina, R. A. Akasov, D. A. Khochenkov, N. A. Arkharova, A. V. Nechaev, E. V. Khaydukov and A. N. Generalova, *Biomater. Sci.*, 2020, **8**, 4570–4580.
85 S. Yan, X. Zeng, Y. A. Tang, B. F. Liu, Y. Wang and X. Liu, *Adv. Mater.*, 2019, **31**, 1905825.
86 M. Cheng, T. Jin, Z. Zhang, Y. Ren, R. Zhang, Y. Wu, Z. Yao and H. Zhang, *ACS Appl. Nano Mater.*, 2023, **6**, 8819–8830.
87 N. Akhtar, C. L. Chen and S. Chattopadhyay, *Biomater. Adv.*, 2022, **141**, 213117.
88 A. Balhara, S. K. Gupta, K. Sudarshan, S. Patra, A. Chakraborty and S. Chakraborty, *ACS Appl. Bio Mater.*, 2024, **7**, 2354–2366.
89 J. Santelli, C. Lepoix, S. Lechevallier, C. Martinez, D. Calise, Q. Zou, S. Moyano, D. Cussac, M. Verelst and R. Mauricot, *Part. Part. Syst. Charact.*, 2021, **38**, 2000216.
90 S. Zha, K. L. Wong and A. H. All, *Adv. Healthcare Mater.*, 2022, **11**, 2102610.
91 S. Zha, H. Liu, H. Li, H. Li, K.-L. Wong and A. H. All, *ACS Nano*, 2024, **18**, 1820–1845.
92 D. B. L. Teh, A. Prasad, W. Jiang, N. Zhang, Y. Wu, H. Yang, S. Han, Z. Yi, Y. Yeo and T. Ishizuka, *NeuroMol. Med.*, 2020, **22**, 139–149.
93 Z. Yi, A. H. All and X. Liu, *Adv. Exp. Med. Biol.*, 2021, **1293**, 641–657.